Theor Chem Acc (2009) 123:273–286
DOI 10.1007/s00214-009-0527-y

REGULAR ARTICLE

Three-dimensional diabatic models for the $\pi\pi^* \rightarrow n\pi^*$ excited-state decay of uracil derivatives in solution

Fabrizio Santoro · Roberto Improta · Vincenzo Barone

Received: 25 November 2008 / Accepted: 2 February 2009 / Published online: 22 February 2009

Abstract Uracil and its derivatives strongly absorb UV light but photodamage is hampered through effective non-adiabatic decay channels. As a first step towards a quantum dynamical (QD) study of the decay route of the photo-excited $\pi\pi^*$ state to the underlying $n\pi^*$ state, here we present our procedure to build a reliable reduced-dimensionality model of the decay process, and we discuss its theoretical foundation. We established the three most important nuclear coordinates for the decay process and we computed the S_1 and S_2 excited-state potential energy surfaces of Uracil and 5-fluoro-Uracil in acetonitrile and in water at TD-DFT level, describing the solvent in the frame of polarizable continuum model. Through a property-based diabatization we obtained the diabatic $\pi\pi^*$ and $n\pi^*$ states' energies and coupling and we fitted them to analytical functions of the nuclear coordinates. We show how these diabatic models can be utilized for QD simulations of the $\pi\pi^* \rightarrow n\pi^*$ decay.

Keywords Uracil · Photoexcitation · Non-adiabatic decay · Potential energy surfaces · Quantum dynamics

Dedicated to the memory of Professor Oriano Salvetti and published as part of the Salvetti Memorial Issue.

F. Santoro (✉) · V. Barone
Istituto per i Processi Chimico-Fisici, CNR,
Area della Ricerca del CNR Via Moruzzi,1, 56124 Pisa, Italy
e-mail: f.santoro@ipcf.cnr.it

R. Improta
Dipartimento di Chimica and INSTM-Village,
Università Federico II, Complesso Monte S. Angelo,
via Cintia, 80126 Naples, Italy

R. Improta
IBB-CNR, via Mezzocannone 16, 80134 Naples, Italy

1 Introduction

In the last decade time-resolved ultrafast spectroscopic techniques have known impressive advances [1, 2], leading to the development of new research fields, such as femto-chemistry, devoted to the understanding and to the control of the elementary excited-state reactive chemical processes [3]. Pump and probe time-resolved absorption and fluorescence spectroscopies have opened the route to the real-time investigation of ultrafast reactive processes, providing fundamental hints on many chemical processes of biological and technological interest [1, 2].

However, especially when dealing with complex systems in their electronic excited states, the interpretation of the experimental results is seldom easy and straightforward. Indeed, suitable theoretical models are often necessary in order to translate the outcome of experiments in terms of chemical 'information', and to unveil the interplay of the several subtle chemical-physical effects ruling the statical and dynamical behavior of the species under study.

As a consequence, femtochemistry is receiving many important benefits by ongoing developments of theoretical methods for the characterization of electronic excited states [4–6]. It is now possible to obtain accurate static descriptions of the potential energy surfaces (PES) of the excited electronic states, also for medium size molecules, in solution and in complex environments (e.g., a protein), as well as to properly include vibrational effects in the description of absorption and emission processes [7–10]. However, although statical quantum mechanical calculations have

provided valuable information for the interpretation of time-resolved experiments [11], a direct comparison between experiments and computations requires a dynamical description.

This is particularly true in the field of ultrafast processes started or even driven by laser pulses [12]. In the latter situation, stationary states simply do not exist since the molecule is governed by a time-dependent Hamiltonian [13]. Especially when dealing with close lying strongly vibronically coupled excited states, in the presence of a laser field, a proper quantum dynamics (QD) treatment becomes mandatory.

Two challenging difficulties limit the possibility of such a fully quantum mechanical (QM) approach. The first problem is the exponential increase of the computational burden of quantum propagations on non-adiabatic systems with the number of nuclear coordinates to be taken into account. This is still a severe issue for sizeable molecules, even if remarkable advances have been made possible by the multiconfigurational description of the wavepacket adopted in MCTDH approach [14–16]. The second problem is maybe even more stringent and is the need for predetermined electronic PESs over the whole space of the nuclear coordinates that will be spanned by the dynamics. The computational time for a full ab initio determination of these PES scales as N^p (where p is the number of nuclear coordinates and N the number of considered points for each coordinate) and this limits the possible application to few degrees of freedom. Both limitations require the definition of reduced-dimensionality models (i.e., in a reduced number of nuclear dimensions) for the system under investigation.

Beyond being dictated by technical difficulties, reduced dimensionality models, which nonetheless encompass most of the physics of the system, are very attractive for interpretative reasons, allowing a simple description of the process and a better understanding of the main effects coming into play. However, reducing the dimensionality of the process under investigation can be a severe approximation. Alternatively, it is possible to resort to classical (CD) or semi-classical (SCD) [17] computations based on the motion of bunches of trajectories released on the excited surface with suitable initial conditions. In these cases the quantum-mechanical event of the transition between different states can be simulated by hopping mechanisms whose probability is ruled by suitable criteria [18]. CD methods scale better with the dimension of the system and can be performed "on the fly" computing for each trajectory energy and forces at each propagation step [19, 20]. An interesting approach, referred to as AIMS (ab initio multiple spawning), has been proposed by Martinez et al. allowing for the introduction of quantum effects in on-the-fly propagations, by expanding the nuclear wavefunction on a adaptive set of classically moving gaussian functions [21]. While on-the-fly CD approaches can be applied straightforwardly also to sizeable systems, it must be recognized that in these cases two possible drawbacks come into play: on the one hand it may be necessary to rely on less accurate electronic descriptions, on the other hand the computations may be so expensive to allow running only a too reduced number of trajectories. Limited bunches of trajectories cannot adequately sample the wave packet and this hampers the description of the dynamical process, especially in the common cases of non-adiabatic transitions at linear or multidimensional conical intersection where, classically speaking, the specific geometry at which the hop takes place may rule the reaction yield. Furthermore, though in many cases SCD and QD simulations lead to similar results [22], mainly for moderate couplings [23], it has been shown that a CD description can diverge from the QD one, for example in cases where the excited state PES is characterized by a wide plateau, which is a common feature in π-delocalized systems [24, 25].

On the ground of these considerations, it is clear that, together with performing all coordinates on the fly CD computations, pursuing full QD studies on suitable models of restricted dimensionality is necessary for a reliable description of the phenomenon under investigation. In order to apply this approach to large size molecules in solution, it is necessary that several methodological questions are assessed. As a step in this direction, we here report the methodological foundations of our study of the dynamics of the two lowest energy excited states of uracil derivatives.

The study of the excited state dynamics of DNA and its constituents has recently emerged as a key topic, because of its many fundamental biological, biomedical and technological implications [26–42]. Indeed DNA strongly absorbs ultraviolet (UV) light and many DNA photolesions originate from singlet excited electronic states (photodamage) [26, 27]. One of the most recent discoveries in the field concerns the decay of the lowest energy bright excited state (S_π) in uracil derivatives. Many investigations have been devoted to the static description of the U decay channels. A direct, barrierless $S_\pi \rightarrow S_0$ decay channel has been individuated and it has been recognized as the responsible for the U ultrafast decay 100–300 fs [28–34]. Recent transient absorption experiments have shown that a second decay channel exists and that a significant part of the population of S_π ($\sim$30%) decays to a long living dark state, which is not the triplet, whose lifetime in aqueous solution is in the picosecond time-scale (τ_s = 24 ps) [35, 36].

Previous static QM studies of ours indicate that this state can be assigned to the lowest energy $n \rightarrow \pi^*$ transition (hereafter S_n) which, according to gas phase computations is more stable than S_π in the Franck–Condon (FC) region [31–34]. The S_n decay channel is available for uracil (U) in all

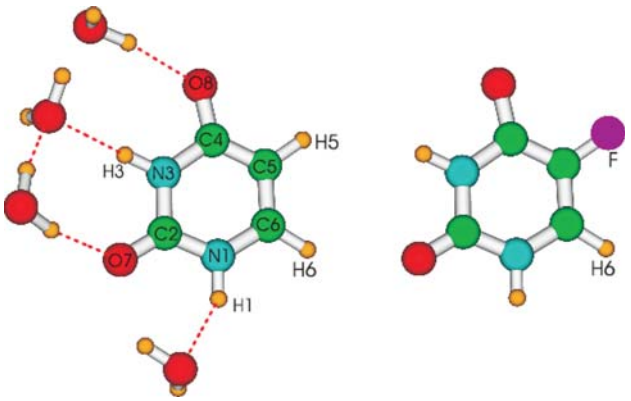

Fig. 1 Schematic description (and atom labeling) of U · $4H_2O$ (*left*) and 5FU (*right*)

the polar solvents, whereas for some of its derivatives, like 5 Fluoro-uracil (5FU), it should occur in polar solvents like acetronitrile but not in water [32, 33]. In a previous paper, based on CASPT2 results in gas phase and TD-DFT results in solution, some of us have investigated the mechanism of ground state recovery from the S_n state, proposing that it does not go through a direct $S_n \rightarrow S_0$ decay, since the corresponding conical intersection lies too high in energy, but it takes place by a mediated $S_n \rightarrow S_\pi \rightarrow S_0$ decay [37].

The non-adiabatic $S_\pi \rightarrow S_n$ population transfer is an inherently quantum mechanical process due to the strong coupling of nuclei and electrons motions in close vicinity of the conical intersection. Looking for a direct comparison with time-resolved (TR) experiments [35, 36], we have thus performed a QM dynamical study of the $S_\pi \rightarrow S_n$ population transfer for U and 5FU in two different solvents (water and acetonitrile). Our theoretical procedure is discussed in the present paper, while a detailed analysis of the QD results and their chemical and physical implications is reported in a parallel study [43].

Bulk solvent effects have been taken into account by the Polarizable Continuum Model (PCM) [44, 45]. While PCM can adequately model CH_3CN solution, a proper description of solvent shifts in aqueous solution requires also the explicit inclusion of water molecules belonging to the first solvation shell. Taking into account experimental [46, 47] and computational [48] evidences all the PCM calculations for aqueous solution refer to the species U · 4 H_20, where four water molecules of the first solvation shell are explicitly included in our model (see Fig. 1).

2 Theoretical methodology

2.1 Selection of the relevant coordinates

The systems under study contain either 12 or 24 atoms (i.e., 30–66 nuclear degrees of freedom) in the condensed phase, and the overall process under investigation involves three different electronic states. As anticipated in the Introduction, a full QD treatment of all the nuclear degrees of freedom is not yet feasible. It is thus necessary to select what are the relevant degrees of freedom to be included in our calculations.

A solid approach to the definition of reduced dimensionality models has been provided by Cederbaum et al. [49] who recently tackled the general problem of the quantum mechanical description of dynamics around a conical intersection in macrosystems. These authors have shown that the Hamiltonian of the system can be transformed in a hierarchy of effective Hamiltonians and that the short time dynamics is ruled by only the first members of this hierarchic series. For two coupled diabatic PESs and considering all the modes on the same footing (no distinction between system and bath) the first member of this hierarchy is a three-dimensional (3D) Hamiltonian, i.e., depending on only three nuclear coordinates, which physically describe (though they may need re-orthogonalization) respectively the motion from a reference geometry to the minima of the two PESs (the diagonal terms of the model) and their coupling (the off-diagonal term). In the present work we work in a similar spirit and define a 3D model for our calculations, where each coordinate is a linear combination of mass-weighted normal coordinates (**Q**) of the ground state S_0, determined by a standard frequency calculation in solution.

As a first step of our analysis, we determined the equilibrium structures of S_1 and S_2 adiabatic states. A first minimum structure located on the S_1 state has a planar geometry. At this structure, here after referred to S_n-min, S_1 is almost completely dark and it corresponds to a HOMO-1 → LUMO excitation, i.e., a $n\pi^*$ transition from the lone pair of oxygen O_8 (S_n in the diabatic description, see below). The most relevant geometry shifts with respect to the ground state minimum S_0-min (i.e., the FC structure) involve the C_4–O_8 and C_5–C_6 bond lengths that increase by 0.1 and 0.04 Å, respectively. A second minimum is found on the S_2 adiabatic state, in the following labeled S_π-min, corresponding to a bright HOMO–LUMO $\pi\pi^*$ transition (S_π in the diabatic description, see below). The most relevant displacements with respect to the FC point are exhibited by the C_4–C_5 (~ -0.03 Å), C_4–O_8 ($\sim +0.03$ Å), and, especially, the C_5–C_6 bond (increasing by ~ 0.1 Å) lengths. Although in the absolute S_2 minimum (S_π-min), the pyrimidine ring is significantly "puckered", experiments [50] and computations [34] suggest that in the first femtoseconds after the excitation on S_2, uracil-like molecules keep the planar geometry they have at the FC point. We have thus optimized the geometry of the S_2 state constraining the pyrimidine ring to planarity (S_π-min^{pla}).

After locating the minima, we analyzed what displacements along the normal coordinates **Q** are necessary to

reach them starting from the FC point. We group the normal modes in two different collective coordinates, q_n and q_π. The former leads towards the S_1 equilibrium structure (corresponding to the S_n minimum after diabatization), the latter to the S_2 minimum S_π-min^{pla} (corresponding to the S_π minimum after diabatization). The definition of the q_n and q_π coordinates (and of the coupling coordinate q_c) in terms of combination of normal coordinates is given in Tables 1, 2 and 3 for U in CH_3CN, 5FU in CH_3CN and U · $4H_2O$ in water, respectively. The contributing normal modes for U in CH_3CN are sketched in Fig. 2. For q_n, Q_{25} corresponds mainly the C_4–O_8 stretch coupled with some H_3 in plane bending, while Q_{26} is essentially the C_2–O_6 stretch; for q_π, Q_{24} corresponds mainly the C_5–C_6 stretch, while Q_{19} and Q_{20} mainly involve ring deformation leading to even more evident coupled bending motions of the H_1, H_3, H_5 and H_6 hydrogen atoms.

Table 1 Definition of the q_c, q_n and q_π coordinates for the 3D model of U in CH_3CN, as combination of the S_0 mass-weighted normal coordinates **Q**

Normal modes								
q_c			q_n			q_π		
Index	ω	δ	Index	ω	δ	Index	ω	δ
Q_{14}	986.5	1.0	Q_{25}	1805.4	−1.980	Q_{19}	1258.2	−0.609
			Q_{26}	1851.0	0.893	Q_{20}	1406.1	−0.588
						Q_{24}	1712.2	−1.051
$q_{c'}$								
Q_{10}	737.3	1.0						

For each coordinate the partecipating normal modes are given together with their S_0 frequencies ω (cm^{-1}) and the (non-normalized) coefficients of the combination. For q_n and q_π these coefficients represent the dimensionless displacements δ along the corresponding normal coordinates from S_0-min to S_n-min and S_π-min^{pla}, respectively. An alternative 3D model was built by adopting the same definition for q_n and q_π and substituting q_c with $q_{c'}$

Table 2 Definition of the q_c, q_n and q_π coordinates for the 3D model of 5FU in CH_3CN, as combination of the S_0 mass-weighted normal coordinates **Q**

Normal modes								
q_c			q_n			q_π		
Index	ω	δ	Index	ω	δ	Index	ω	δ
Q_{16}	908.8	1.0	Q_{26}	1812.4	−1.920	Q_{21}	1376.4	0.889
			Q_{27}	1853.4	1.014	Q_{25}	1758.6	0.965

For each coordinate the partecipating normal modes are given together with their S_0 frequencies ω (cm^{-1}) and the (non-normalized) coefficients of the combination. For q_n and q_π these coefficients represent the dimensionless displacements δ along the corresponding normal coordinates from S_0-min to S_n-min and S_π-min^{pla}, respectively

In our definition of the q_n and q_π coordinates we neglect modes showing a small displacement, and those with a too low frequency (<800 cm^{-1}). This latter choice emphasizes the description of the ultrafast part of the process within a simple 3D model, without unphysically constraining modes with inherently different frequencies (i.e., accelerations in an harmonic model) to move simultaneously. Naming ΔQ_n and ΔQ_π the vectors of the displacements from S_0-min to S_n-min and S_π-min^{pla}, the two coordinates q_n and q_π are represented by the two unit vectors $\overrightarrow{q_n} = \sum_i \overrightarrow{Q_i}\Delta Q_i^n / \sqrt{\sum_i (\Delta Q_i^n)^2}$ and $\overrightarrow{q_\pi} = \sum_i \overrightarrow{Q_i}\Delta Q_i^\pi / \sqrt{\sum_i (\Delta Q_i^\pi)^2}$. As reported in the next section we have combined the S_1 and S_2 adiabatic states to obtain two diabatic states, one bright (S_π) and the other dark (S_n) with respect to the ground state S_0.

A 2D scan of the S_1 and S_2 PESs along the q_n and q_π coordinates, followed by diabatization and analytical fit of the PESs allows to determine the line of degeneracy (intersection) of the two adiabatic (diabatic) surfaces and its minimum (the minimum energy conical intersection, CI^{min} in our model)

The diabatic states S_n and S_π belong to different symmetries in C_s (namely A'' and A' respectively), therefore, their coupling is vanishing. As a consequence the third "coupling" coordinate q_c of our 3D model must be an out-of-plane (A'') vibrational mode.

Using U as reference compound, we performed a three-points monodimensional scan along each out-of-plane normal coordinate around the CI^{min} structure and, after diabatization (see next section), we obtained the derivative of the coupling along each normal coordinate. For the systems in acetonitrile (computationally more affordable) we checked the computation of the derivatives (specifically its constancy around CI^{min}) by extending the scan to seven points along each coordinate. The larger is such derivative (for dimensionless normal coordinates) the more the mode is expected to play a role in the non-adiabatic decay. At variance with the Cederbaum's approach (who considered the coupling coordinate obtained by the linear combination of all the modes each weighted for the corresponding derivative of the coupling), we worked out different 3D models, mostly adopting a single mode for our definition of q_c, to investigate the dependency of the dynamical simulation on the specific nuclear motion, and to obtain a simpler and clear cut interpretation of the $S_\pi \rightarrow S_n$ decay mechanism.

For what concerns uracil in CH_3CN, Fig. 3 reports the computation around the CI^{min} which has coordinates $\{-0.13, 0.62\}$ bohr × amu$^{1/2}$ in the $\{q_n, q_\pi\}$ plane. It is apparent that Q_{14} is the S_0 normal coordinate producing the largest diabatic coupling. On S_0 it has a frequency

Table 3 Definition of the q_c, q_n and q_π coordinates for the 3D model of U · $4H_2O$ in water, as combination of the S_0 mass-weighted normal coordinates **Q**

Normal modes								
q_c			q_n			q_π		
Index	ω	δ	Index	ω	δ	Index	ω	δ
Q_{38}	1009	1.0	Q_{45}	1476.4	0.546	Q_{33}	807.0	0.891
			Q_{46}	1523.2	−0.816	Q_{41}	1122.3	−0.549
			Q_{51}	1723.4	0.721	Q_{43}	1280.7	0.633
			Q_{52}	1741.2	1.319	Q_{44}	1419.9	−0.481
			Q_{53}	1753.8	1.503	Q_{50}	1701.4	0.591
						Q_{54}	1800.0	0.591
$q_{c'}$								
Q_{31}	734.0	1.0						
$q_{c''}$								
Q_{34}	813.3	1.0						
$q_{c'''}$								
Q_{31}	734.0	−2.423						
Q_{34}	813.3	1.254						

For each coordinate the contributing normal modes are given together with their S_0 frequencies ω (cm^{-1}) and the (non-normalized) coefficients of the combination. For q_n and q_π these coefficients represent the dimensionless displacements δ along the corresponding normal coordinates from S_0-min to S_n-min and S_π-min^{pla}, respectively. Alternative 3D models were built by adopting the same definition for q_n and q_π and substituting q_c with $q_{c'}$, $q_{c''}$ and $q_{c'''}$, respectively

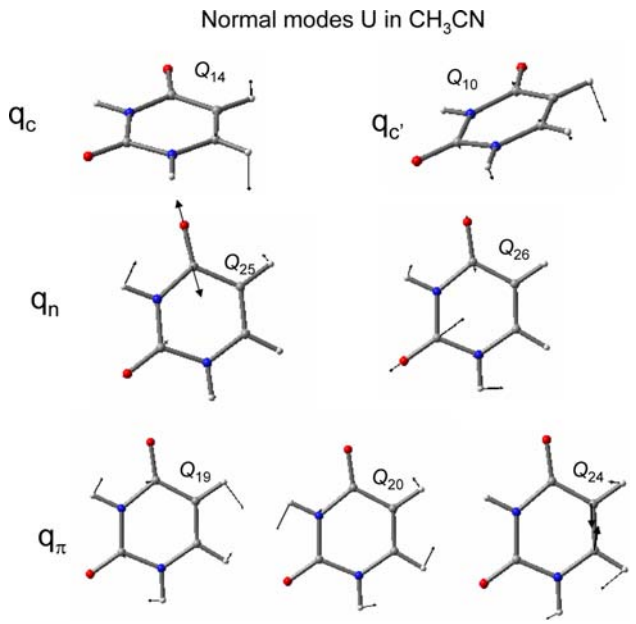

Fig. 2 Schematic description of the normal modes contributing to coordinates adopted in the 3D model of U in CH_3CN

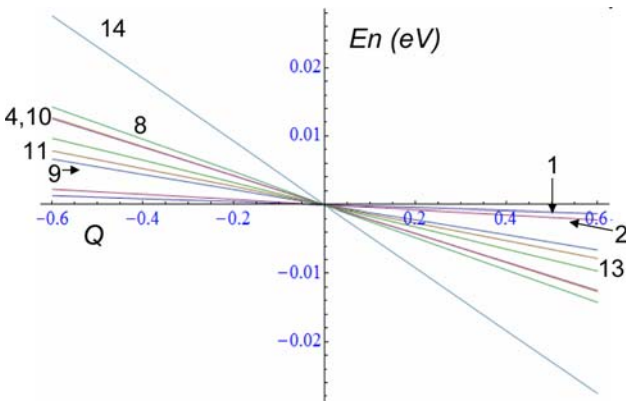

Fig. 3 1D scans of the diabatic coupling for U in CH_3CN as a function of the 9 non-planar A'' dimensionless normal coordinates

$\nu = 986.5\ cm^{-1}$, and represents an out of phase out of plane motion of H_6, mainly, and H_5. Its derivative is almost twice larger than that of the other modes.

In water the situation is more complex. In fact, because of the presence of the first solvation shell, the system cannot exhibit a pure C_s symmetry, since some of the hydrogen atoms of the water molecules cannot lie either in the molecular ring or be disposed symmetrically with respect to it. As a consequence, the coupling is not vanishing also when the nucleobase geometry is perfectly planar, and vibrational modes preserving the base planarity can also affect the coupling. Furthermore, besides the intramolecular degrees of freedom, also vibrational modes mainly involving the water molecules of the first solvation shell can act as coupling modes.

Not surprisingly, our analysis thus indicates that in water there are several modes with comparable coupling strength

(derivatives), and many of them involve the motion of water molecules.

In order to reduce the bias that the choice of the solvation shell can have on the results, we adopt a 'conservative' approach, focussing on the intra-base degrees of freedom. We want indeed to be sure of not overestimating the dynamical solvent effect of the first solvation shell molecules, since it cannot be taken for granted that the dynamical effect of the outer solvation shells on their dynamics is correctly reproduced by PCM.

Among the solute vibrational modes we then selected those that are more similar to the coupling mode obtained for U in CH_3CN. Indeed, not only in CH_3CN the system is simpler and our procedure safer and more accurate, but in this way the results obtained in the two solvents are more directly comparable.

On this ground, we chose as coupling vibrational modes in water the normal modes Q_{34} (in phase out of plane of H_5, mainly, and H_6, $\nu = 813$ cm^{-1} on S_0) and Q_{38} (out of phase out of plane motion of H_6, mainly, H_5 and H_1, $\nu = 1008$ cm^{-1} on S_0). For additional tests we also worked out different models adopting as a coupling mode Q_{31} and a combination of Q_{31} and Q_{34}, leading toward the absolute non-planar minimum S_π-min.

Finally, in analogy with what found for U, we selected as coupling mode for 5FU in CH_3CN the vibrational mode 16, with $\nu = 908$ cm^{-1}, corresponding to the out of plane motion of H_6.

Once the three coordinates were established for the investigated systems, we performed an extended 3D scan of their S_1 and S_2 PESs on a grid of points. By performing at each point of the grid the diabatic transformation, we obtained the diabatic diagonal potentials V_π and V_n and the coupling $V_{n\pi}$, and we fitted them to analytical functions. It is important to highlight that by this approach we go beyond the classical linear coupling model [49] (sometimes known as multi-mode vibronic-coupling approach) [51], inasmuch anharmonicities are considered on V_π and V_n, and $V_{n\pi}$ is not confined to be a linear function of the coupling coordinate. Indeed the coupling $V_{n\pi}$ turns out to be a more complex function of the nuclear coordinates and, in its power expansion, cross terms in q_π and q_c and mostly in q_n and q_c play a relevant role (see the result section).

2.2 Diabatization procedure

Born–Oppenheimer (BO) adiabatic states are coupled by non-adiabatic couplings deriving from the action of nuclear kinetic operator on the electronic wavefunctions. Since these couplings vary sharply with the nuclear coordinates and are difficult to be treated [51], quantum dynamics is usually computed on a diabatic model, where diabatic states are defined so to be weakly dependent on nuclear coordinates (ideally independent). Accordingly, non-adiabatic kinetic couplings become negligible, while a potential coupling between the two diabatic states arises. This coupling is a smooth function of nuclear coordinate and is, therefore, more suitable for calculations. Different methodologies have been proposed to define "diabatic states" [52]. We rely on a property-based methodology, where the two diabatic states are defined imposing a pre-determined behaviour in the dependence of a one-electron property on nuclear coordinates, so to minimize the configurational change of the electronic wavefunctions (which is the origin of large non-adiabatic kinetic couplings). To fix the ideas consider U in CH_3CN. The S_0 equilibrium structure is planar (C_s symmetry). In this symmetry states coming from $\pi\pi^*$ and $n\pi^*$ excitation belong to different representations, A' and A'' respectively, and therefore, are not coupled. Assuming xy to be the molecular plane, the transition dipole moment $S_0 \rightarrow \pi\pi^*$ has non-vanishing x and y components while the $S_0 \rightarrow n\pi^*$ is weak and polarized along the z axis. At non-planar geometries the two $\pi\pi^*$ and $n\pi^*$ states are coupled, and the resulting adiabatic S_1 and S_2 states both bring some oscillator strength in the xy plane with the ground state S_0. We define the two diabatic states S_π and S_n by rotating the transition dipole moment matrix (in the S_1, S_2 adiabatic basis) so to have a bright diabatic state S_π (i.e., $\pi\pi^*$) which concentrates all the xy oscillator strength with S_0 and a second state S_n (i.e., $n\pi^*$) which is dark for xy-polarized transitions from S_0 (z-polarized transitions are yet possible but very weak and they will be neglected in the following). Consider the raw vector of the basis set of the first three adiabatic states ($|S_0\rangle$, $|S_1\rangle$, $|S_2\rangle$), our TD-DFT calculations provide us at each point of the grid the adiabatic electronic Hamiltonian $\mathbf{H}_{\mathrm{ad}}$ and transition dipole matrix $\mathbf{M}_{\mathrm{ad}}$

$$\mathbf{H}_{\mathrm{ad}} = \mathrm{diag}(E_{00}, E_{11}, E_{22}) \tag{1}$$

$$\mathbf{M}_{\mathrm{ad}} = \begin{pmatrix} \mu_{00} & \mu_{01} & \mu_{02} \\ \mu_{01} & \mu_{11} & \mu_{12} \\ \mu_{02} & \mu_{12} & \mu_{22} \end{pmatrix} \tag{2}$$

We rotate our adiabatic basis set in order to obtain a diabatic basis set whose two excited states are either bright (S_π) or completely dark (S_n), with respect to the ground state S_0. Notice that the linear-response TD-DFT calculations we performed cannot provide the value μ_{12}, and a quadratic response approach should be implemeted. However, it easy to realize that this value is not needed for our diabatization scheme. In formulae, naming ($|S_0\rangle$, $|S_n\rangle$, $|S_\pi\rangle$) the diabatic set, we have

$$(|S_0\rangle, |S_n\rangle, |S_\pi\rangle) = (|S_0\rangle, |S_1\rangle, |S_2\rangle)\mathbf{C}^T \tag{3}$$

and we obtain the orthonormal transformation $\mathbf{C}$ imposing that S_0 is left unaltered,

$$\mathbf{C} = \begin{pmatrix} 1 & 0 & 0 \\ 0 & \cos(\theta) & \sin(\theta) \\ 0 & -\sin(\theta) & \cos(\theta) \end{pmatrix} \quad (4)$$

and that in the diabatic dipole matrix

$$\mathbf{M}_d = \mathbf{C}\mathbf{M}_{\mathrm{ad}}\mathbf{C}^T = \begin{pmatrix} \mu_{00} & \mu_{0n} & \mu_{0\pi} \\ \mu_{0n} & \mu_{nn} & \mu_{n\pi} \\ \mu_{0\pi} & \mu_{n\pi} & \mu_{\pi\pi} \end{pmatrix} \quad (5)$$

$\mu_{0n} = 0$ and $\mu_{0\pi} \neq 0$.

With this procedure we obtain the diabatic PESs V_π and V_n and their coupling $V_{n\pi}$ in the points of the grid utilized for ab initio computations

$$\mathbf{H}_d = \mathbf{C}\mathbf{H}_{\mathrm{ad}}\mathbf{C}^T = \begin{pmatrix} E_{00} & 0 & 0 \\ 0 & V_n & V_{n\pi} \\ 0 & V_{n\pi} & V_\pi \end{pmatrix} \quad (6)$$

For Ur in CH_3CN we chose a $9 \times 20 \times 24$ 3D grid of equally spaced points in the $\{q_c, q_n, q_\pi\}$ space with boundaries: $-0.314507 \leq q_c \leq 0.943503$, $-0.31998 \leq q_n \leq 1.1999$ and $-0.215874 \leq q_\pi \leq 1.02538$. For 5FU in CH_3CN the grid was $9 \times 20 \times 24$ $-0.228203 \leq q_c \leq 0.68461$, $-0.319113 \leq q_n \leq 1.19664$, $-0.208402 \leq q_\pi \leq 0.989913$. Finally, for the more computationally demanding U in water (the solute is $U \cdot 4H_2O$) the grid is $9 \times 17 \times 22$ with $-0.259176 \leq q_c \leq 0.777528$, $-0.356332 \leq q_n \leq 1.06901$, $-0.212036 \leq q_\pi \leq 0.90116$. All the coordinates are expressed in bohr $\times$ amu$^{1/2}$.

2.3 Treatment of solvent effect

When discussing dynamical processes in solution, it is important that solvent relaxation time is taken into the proper account. In fact a finite time is required for the complete equilibration of the solvent reaction field when the solute electronic state (and, thus, its electron density) changes. Although more complex schemes can be envisaged [53], within the framework of continuum solvation models a simple approach to dynamical solvation effects relies on the decomposition of the solvent degrees of freedom in two components: fast/electronic and slow/nuclear. Only the fast component equilibrates instantaneously to the solute electron density. On this ground it is possible to define two limit situations, usually referred to as non-equilibrium (neq) and equilibrium (eq) time-regimes. In the former case, only solvent electronic polarization (fast solvent degrees of freedom) is in equilibrium with the excited-state electron density of the solute, whereas in the equilibrium regime also nuclear polarization (and, thus, both fast and slow solvent degrees of freedom) is equilibrated with the excited-state electron density.

In the framework of continuum solvation models the two situations are ruled by two different dielectric constants. In the non-equilibrium case, the reaction field due to the fast solvent degrees of freedom depends on the dielectric constant at optical frequency ($\varepsilon_{\mathrm{opt}}$, usually related to the square of the solvent refractive index n, $\varepsilon_{\mathrm{opt}} = n^2$, 1.776 for water and 1.8006 for CH_3CN). Equilibrium solvation is instead ruled by the static dielectric constant.

It is clear that in order to investigate the ultrafast dynamics in the FC region non-equilibrium solvation energies are more suitable, and therefore, our PESs have been built by equilibrating the fast degrees of freedom to the S_π and S_n excited states, but leaving the slow degrees of freedom always equilibrated with S_0. Obviously, this approximation is strictly valid only at the FC point. While the system moves on the S_π surface, slow solvent degrees of freedom start equilibrating with S_π density, and this process is expected to modulate the S_π–S_n energy gap, the position of the CI and the system dynamics. When these effects are expected to be important, solvent dynamics should be explicitly take into account, within the same framework used by Hynes et al. to treat Conical Intersections in solution [54].

However, as shown below, the $S_\pi \rightarrow S_n$ population transfer occurs on a ultrafast time scale ($\sim$50 fs) and thus a non-equilibrium approach is expected to be fully reliable.

Furthermore, it must be noticed that explicit inclusion of solvation degrees of freedom within the dynamical treatment is particularly important for studying the interaction of electronic states with strongly different electron density (as, e.g., when charge transfer states are involved). This is not the case of the lowest energy electronic states of uracil derivatives. In order to put these considerations on a quantitative basis, we have computed (at TD-DFT level, see next section for details) the (eq) and (neq) energy of S_n and S_π for U in CH_3CN. Equilibration of the slow degrees of freedom leads to a stabilization of $\sim$0.35 eV for S_n, and of only $\sim$0.1 eV for S_π. Furthermore, experiments on Coumarin C153 indicate that the total relaxation of solvent degrees of freedom occurs on $a \sim ps$ time scale [55], which is significantly longer than the one investigated here. Solvent equilibration is thus expected to play some role in S_n-min, contributing to the energy dissipation and decreasing the probability of $S_n \rightarrow S_\pi$ back transitions, but its influence on the ultrafast part of the excited state decay is small. For what concerns the calculations in aqueous solution, the first solvation shell is included in our model, further decreasing the importance of taking into account dynamical solvent effects (computed within the framework of a continuum solvation model) in our treatment.

In this respect, it is important to remind that, though PCM can take care of the influence of the outer solvation shell on the static properties of our system, it probably underestimates the dynamical restraints due to the presence

of hydrogen bonds between the first and the second solvation shell. In this case, semi-classical dynamics including a large number of explicit water molecules (even if treated at the molecular mechanics level) could provide useful hints for evaluating the dynamical solvent effect on the excited state dynamics.

2.4 Selection of the electronic method

In the present study, the adiabatic PESs and the diabatic coupling have been built at the TD-DFT level [56, 57], adopting the PBE0 functional [58–60]. As anticipated above, bulk solvent effects have been included by means of PCM. We choose this approach for several reasons. First, the limited cost of our computational approach has allowed an extensive explorations of the S_1 and S_2 adiabatic states. This is an important advantage since in principle the kinetic energy acquired through photoexcitation may allow the system to move in a large domain of the coordinate space and obviously it is necessary to characterize the PESs in this whole domain.

Furthermore, since the outcome of the QD calculations critically depends on the quality of the PES, it is important to rely on methods able to provide a good description of the FC region and of the relevant minima. In this respect PCM/TD-PBE0 is able to compute accurate vertical excitation energies (VEE) and emission energies in solution of uracil derivatives [33, 34, 39]. The overall shape of the excited state PES accessible to the wavepacket should also be reliably described. In fact the dynamics is obviously ruled by PESs shapes that set the initial acceleration along each vibrational mode, as well as they govern intramolecular energy redistribution (through couplings). Moreover, the position and shape of the conical intersection between different electronic states deeply affect the non-adiabatic population transfer that is the phenomenon we want to investigate in our systems.

Actually, there are encouraging indications that PCM/TD-PBE0 calculations can fulfill also this latter requirement. In fact, when used to compute the absorption and emission spectra, PCM/TD-PBE0 calculations usually provide accurate vibrational contributions [4–6].

TD-DFT is not expected to reliably treat processes involving a CI with the ground electronic state [61, 62], although very recent studies indicate that a qualitative correct description of excited state decay can be obtained also in this case [63, 64].

On the other hand the intersection between two excited states can be correctly described by TD-DFT. In fact, when applied to the study of the $S_2 \rightarrow S_1$ decay in pyrazine, TD-DFT calculations are in very good agreement with the experimental results and with the predictions based on the most accurate (and available) ab initio methods [65].

2.5 Computational details

Ground and excited geometry optimizations have been performed at the PCM/PBE0/6-31G(d) and at the PCM/TD-PBE0/6-31G(d) level, respectively, using the UATM model (UA0 radii) for the solute cavity [66]. The adiabatic PES have been built by using UAHF radii [66], which are expected to provide more accurate ground state solvation energies. In any case we have checked that our results do not qualitatively change when different cavity radii and more extended basis sets are used [43].

2.5.1 Quantum dynamical calculations

We performed quantum dynamical (QD) calculations on the 3D models by using an in-house developed program. Since the three coordinates (q_n, q_π and q_c) are orthogonal combinations of mass-weighted normal coordinates of the ground electronic state **Q**, the kinetic Hamiltonian has the simple form $\sum_{i=c,n,\pi} -(\hbar^2/2)\partial^2/\partial q_i^2$. We use the Fourier method [67], representing the wave packet on 3D grid of points, and computing the kinetic integrals by fast Fourier transform (FFT). To ensure convergence and stability of the QD simulations according to the Fourier method the V_π, V_n, $V_{n\pi}$ diabatic potentials must be represented on 3D grids more dense and extended than those used for ab initio computations. These grids were generated by using the

Table 4 Diabatic potential energy surfaces (PES) for U in CH_3CN with coupling Q_{14}

Pol. terms	Exp. coeff.		Pol. terms	Exp. coeff
	V_π	V_n		$V_{n\pi}$
E_0	5.39798	4.96477	q_c	−0.108007
q_c^2	0.103352	0.193158	$q_c q_n$	0.0994372
q_c^4	0.129441	0.122416	$q_c q_n^2$	−0.00822225
q_n	−0.581218	−1.57052	$q_c q_n^3$	−0.0257742
$q_c^2 q_n$	0.0606791	0.0896478	$q_c q_n^4$	0.00832508
q_n^2	1.71343	1.55997	$q_c q_\pi$	−0.0126452
$q_c^2 q_n^2$	−0.00666724	−0.0420344	$q_c q_\pi^2$	−0.000545084
q_n^3	−0.729554	−0.263028	$q_c q_\pi^3$	−0.00304319
q_n^4	0.142191	0.0338705	$q_c q_\pi^4$	0.0000477736
q_p	−0.711214	−0.21062		
$q_c^2 q_\pi$	0.0123265	−0.0750758		
$q_n q_\pi$	0.0810826	0.0869156		
q_π^2	1.20355	1.18827		
$q_c^2 q_\pi^2$	0.0141595	0.0175261		
q_π^3	−0.261314	−0.220737		
q_π^4	0.0796964	0.0694905		

Polynomial terms and expansion coefficients for the different PES. Expressing the coordinates in bohr × amu$^{1/2}$, energies in eV are obtained with respect to the S_0 minimum, whose energy is set to zero

Table 5 Diabatic potential energy surfaces (PES) for 5FU in CH_3CN with coupling Q_{16}

Pol. terms	Exp. coeff.		Pol. terms	Exp. coeff
	V_π	V_n		$V_{n\pi}$
E_{00}	5.13480	5.02182	q_c	−0.112202
q_c^2	0.0252691	0.113043	$q_c q_n$	0.0535665
q_c^4	0.221802	0.199018	$q_c q_n^2$	0.0170767
q_n	−0.482917	−1.5598	$q_c q_n^3$	−0.0144699
$q_c^2 q_n$			$q_c q_n^4$	0.00116612
q_n^2	1.80015	1.60671	$q_c q_\pi$	−0.0280078
$q_c^2 q_n^2$			$q_c q_\pi^2$	−0.0164319
q_n^3	−0.576116	−0.328352	$q_c q_\pi^3$	−0.00170137
q_n^4	0.0488106	0.0500528	$q_c q_\pi^4$	−0.00257382
q_p	−0.741519	−0.273264		
$q_c^2 q_\pi$				
$q_n q_\pi$	0.0640382	0.0631348		
q_π^2	1.1967	1.17356		
$q_c^2 q_\pi^2$				
q_π^3	−0.376706	−0.28016		
q_π^4	0.149917	0.0690114		

Polynomial terms and expansion coefficients for the different PES. Expressing the coordinates in bohr × amu$^{1/2}$, energies in eV are obtained with respect to the S_0 minimum, whose energy is set to zero

Table 6 Diabatic potential energy surfaces (PES) for U · $4H_2O$ in water with coupling Q_{38}

Pol. terms	Exp. coeff.		Pol. terms	Exp. coeff
	V_π	V_n		$V_{n\pi}$
E_{00}	5.29223	5.28944	q_c	−0.0918778
q_c^2	0.216541	0.18963	$q_c q_n$	0.0650785
q_c^4	0.0910123	0.142752	$q_c q_n^2$	0.0121379
q_n	−0.528429	−1.30683	$q_c q_n^3$	−0.00984624
$q_c^2 q_n$	0.0434316	−0.00471651	$q_c q_n^4$	−0.00664634
q_n^2	1.15812	1.25497	$q_c q_\pi$	0.0184148
$q_c^2 q_n^2$	0.0343402	0.0490163	$q_c q_n q_\pi$	0.0479667
q_n^3	−0.305648	−0.080076	$q_c\ q_n^3\ q_\pi$	0.0307903
q_n^4	0.0152541	0.0371717	$q_c q_\pi^2$	0.00300773
q_p	−0.655390	−0.311299	$q_c q_\pi^3$	0.00855236
$q_c^2 q_\pi$	−0.0373734	−0.0452886	$q_c q_n q_\pi^3$	−0.0193571
$q_n q_\pi$	0.0831782	0.121334	$q_c q_\pi^3$	0.000753415
q_π^2	1.02679	0.984119		
$q_c^2 q_\pi^2$	0.0927535	0.0660281		
q_π^3	−0.388450	−0.303494		
q_π^4	0.251887	0.140198		

Polynomial terms and expansion coefficients for the different PES. Expressing the coordinates in bohr × amu$^{1/2}$, energies in eV are obtained with respect to the S_0 minimum, whose energy is set to zero

analytical fitting functions reported in Tables 4, 5 and 6. Test calculations have shown that a (64 × 64 × 64) grid with $-2.5 \le q_c \le 2.5$, $-1.6 \le q_n \le 3.0$ and $-1.6 \le q_\pi \le 3.0$ (all coordinates expressed as bohr × amu$^{0.5}$) provides fully converged propagations of the initial wavepacket. We assume a δ (in time) excitation of the system from S_0 to $S\pi$ and the initial vibrational state is chosen to be the harmonic ground state of S_0 along the three coordinates. In the definition of this latter state, frequencies are determined by second-order derivatives of the S_0 PES computed on the same grid of points as S_1 and S_2 and Duschinsky couplings are neglected. The equilibrium geometry of the S_0 is the origin of the $\{q_c, q_n, q_\pi\}$ space and the frequencies in wavenumber are ω_c = 1001.7, 915.7, 1029.4, ω_n = 1846.3, 1847.3, 1723.8, and ω_π = 1529.76, 1517.7, 1415.6 for U in CH_3CN, 5FU in CH_3CN and U in water, respectively. Notice that the S_0 frequencies associated to the coupling q_c coordinates computed according to the 3D model are in very good agreement with those obtained by full-coordinate harmonic analysis (see data in Tables 4, 5 and 6). The time-dependent Schrödinger equation for the wave packet evolution is solved numerically by an orthogonalized-Lanczos method [23, 68], adopting a basis of 21 Lanczos vectors for a time step propagation of 7 au. Convergence with respect to time-step and number of Lanczos vectors has been carefully checked (in typical runs the last Lanczos vector population remains $<10^{-25}$).

3 Results

The methodological approach outlined above has been applied to the explicit study of three different systems, namely U in CH_3CN, 5FU in CH_3CN and U · 4 H_2O in water. The parameters of the fits are reported in Tables 4, 5, 6. The root mean square deviation (RMSD) of the fits of V_π and V_n are 0.01 and 0.009 eV for U · 4 H_2O, 0.01 and 0.006 eV for U in CH_3CN and, 0.008 and 0.006 eV for 5FU in CH_3CN. The RMSDs of the adiabatic S_1 and S_2 energies (obtained by diagonalization of the diabatic Hamiltonian matrix) for the three systems are 0.009, 0.011, 0.007, 0.01, 0.006 and 0.008 eV. These parameters prove that the diabatization and fitting procedures introduce negligible errors on the energies of the 3D model. The further step is to verify whether our 3D reduced dimensionality models provide a good description of the true systems excited state PESs. We have thus located on the computed PES's the minima of S_0, S_n and S_π.

As shown in Table 7, the energy of the minima of the 3D fitted adiabatic PES is in good agreement (within 0.15 eV) with that of the 'full coordinate' ones, i.e., those provided by the PCM/TD-PBE0 geometry optimizations, especially for what concerns the description of the S_n and S_π minima. The only significant difference concerns S_n-min of U · 4 H_2O, that in the 3D model is destabilized by ~0.25 eV. In this case, constraining the solvation shell to

Table 7 Adiabatic energies (in eV, with respect to the S_0 minimum) of S_0, S_n and S_π in the minima S_0-min, S_n-min and S_π-min^{pla}, computed for U in water and in acetonitrile and 5FU in acetonitrile at the PCM/TD-PBE0 level

	FC	S_π-min^{pla}	S_n-min
U in acetonitrile UAHF			
S_0	0 (0)	0.34 (0.17)	0.62 (0.48)
S_n	4.91 (4.96)	4.77 (4.78)	4.42 (4.53)
S_π	5.37 (5.40)	5.10 (5.24)	5.45 (5.47)
U · 4 H_2O in water UAHF			
S_0	0 (0)	0.37 (0.18)	0.68 (0.42)
S_n	5.27 (5.29)	5.15 (5.11)	4.66 (4.92)
$S_\pi S_\pi$	5.27 (5.29)	4.99 (5.13)	5.47 (5.33)
5FU in acetonitrile UAHF			
S_0	0 (0)	0.34 (0.18)	0.61 (0.48)
S_n	4.98 (5.02)	4.89 (4.88)	4.47 (4.59)
S_π	5.12 (5.13)	4.83 (4.98)	5.24 (5.28)

In parenthesis the corresponding energies obtained by the fitted PESs are given

adopt a planar coordination geometry significantly disfavors S_n-min, which is characterized by noticeable rearrangements of the cybotactic region. As a consequence our calculations are expected to somehow underestimate the $S_n \rightarrow S_n$ population transfer. In any case this discrepancy is not expected to qualitatively change our results, as shown by the results obtained by varying the S_n/S_π energy gap [43]. The contour plot of the V_π and V_n potentials for the three analyzed systems are reported in Fig. 4. Recalling that the ground state equilibrium structure is placed at the origin of the coordinate system, as expected, in all the cases the minimum of V_n is more displaced along the coordinate q_n while the minimum of V_π is more displaced along q_π. Nonetheless, interestingly the V_π minimum has also a significant displacement along q_n which means that while the system photoexcited on V_π in the FC region [around the (0, 0, 0) point] moves toward its minimum, also the V_n energy slightly decreases.

Figure 5 reports the 3D plots of V_π and V_n diabatic potentials (left upper panel) of U · 4 H_2O in water in the $\{0, q_n, q_\pi\}$ plane and their coupling $V_{n\pi}$ (right upper panels) in the $\{q_c, q_n, 0\}$ plane. Notice that the coupling $V_{n\pi}$ vanishes for $q_c = 0$ and the crossing line of the two diabatic potentials corresponds to the intersection seam of the two adiabatic surfaces S_1 and S_2, as expected, correctly has dimension 1 in a 3D space. Though, for fixed q_n values the slope of the coupling $V_{n\pi}$ along the coupling q_c coordinate is almost constant, in line with a classical linear model, the plot shows that such a slope has pronounced dependence on q_n, i.e., roughly speaking on the C_4-O_8 stretch, putting into evidence the necessity to go beyond the classical linear coupling model (sometimes known as multi-mode vibronic-coupling approach) [51]. The lower panel of Fig. 5 reports the difference of an harmonic fit (only linear and quadratic terms) of the V_n and V_π potentials of U · 4 H_2O in water with respect to the anharmonic fits reported in Table 6 in the $\{0, q_n, q_\pi\}$ plane. It is apparent that deviation from harmonicity is moderate, and more pronounced for V_π than for V_n.

A detailed analysis of the $S_\pi \rightarrow S_n$ population transfer and of its implications for the DNA photochemistry is reported in a parallel study [43]. Shortly, in all the systems considered, within 50 fs after the excitation there is a substantial ($\sim$0–30 %) population transfer from S_π to S_n, in quantitative agreement with the experimental estimates. Here we discuss in greater detail the effect of the coupling mode on the population transfer to S_n. To this purpose we have performed QD calculations for U in acetonitrile, and for U · 4H_2O in water, adopting different coupling coordinates (reported in Tables 4 and 6, respectively), and the corresponding time evolutions of the S_n population are shown in Fig. 6 (upper panel U in acetonitrile; lower panel U · 4H_2O in water).

Results are reported up to 1 ps after photoexcitation. Nonetheless, since an alternative, direct $S_\pi \rightarrow S_0$ decay channel is operative [28–34] and the decay of S_π population observed experimentally is in the 100–300 fs timescale [33], a population transfer $S_\pi \rightarrow S_0$ can be considered competitive if it takes place in the first $\approx$100 fs. Moreover, on the long timescale of hundreds of fs also non-planar motions, different from that described by the coupling coordinate q_c, can be relevant for the U dynamics, and they are not included in our model. Therefore, while the short-time evolution of the S_n population is realistic for U and proves the feasibility of the S_n decay channel, the long time behavior has mainly a speculative interest (what would be the U dynamics in absence of non-planar motions and of the $S_\pi \rightarrow S_0$ decay channel).

Figure 6 shows that, for U in acetonitrile, the 3D model adopting as coupling coordinate $q_c \equiv Q_{14}$ predicts a fast transfer of about 10 % of the initial S_π population to S_n. At variance, the coupling introduced by coordinate $q_{c'} \equiv Q_{10}$ leads to a negligible transfer of population. In a similar way, for U · 4H_2O in water the mode $q_c \equiv Q_{38}$ induces a fast and remarkable transfer of population to the S_n state and the same is true for $q_{c'} = Q_{34}$ (see Ref. [43]) while negligible S_n population is triggered by $q_{c''}$, i.e., a combination of the Q_{31} and Q_{34} modes, which is physically interesting because it leads toward the non-planar minimum of the S_π surface. The results put into evidence that, as expected, the choice of the coupling coordinate must be performed carefully, since it can drastically effect the outcome of the simulations. This fact highlights something that, though being well recognized in the QD community, is often overlooked in the much wider community

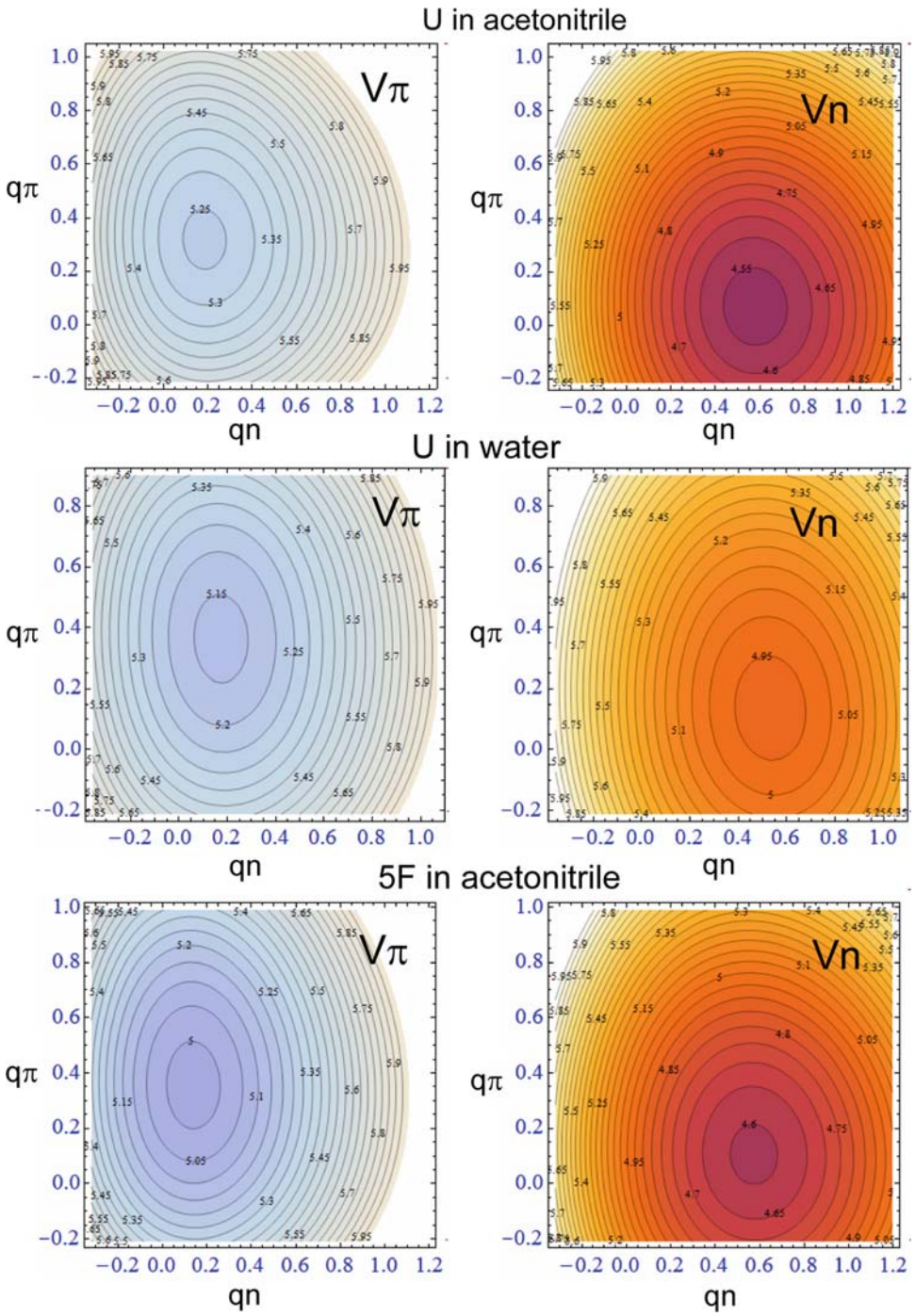

Fig. 4 Contour plots of the V_π (*left*) and V_n (*right*) diabatic potentials for U in CH_3CN (upper panel), U · 4 H_2O in water (*middle*) and 5FU in CH_3CN (*lower*)

interested in photochemistry and photophysics, and specifically that the mere existence of a an accessible conical intersection does not imply an effective non-adiabatic population transfer, since this latter phenomenon does also critically depend on the coupling strength.

The evolution of the S_n population shows strong and not regular oscillations for U both in acetonitrile and in water, and differences emerge between the behaviors in the two solvents. These features reveal the existence of a complex multidimensional non-adiabatic dynamics in U derivatives, and they will be investigated in more detail in a forthcoming article [43].

4 Concluding remarks

We have here described the methodological approach we have followed in order to study the $S_\pi \rightarrow S_n$ population transfer in uracil derivatives by means of QD calculations, establishing a series of 3D models depending on the solvent

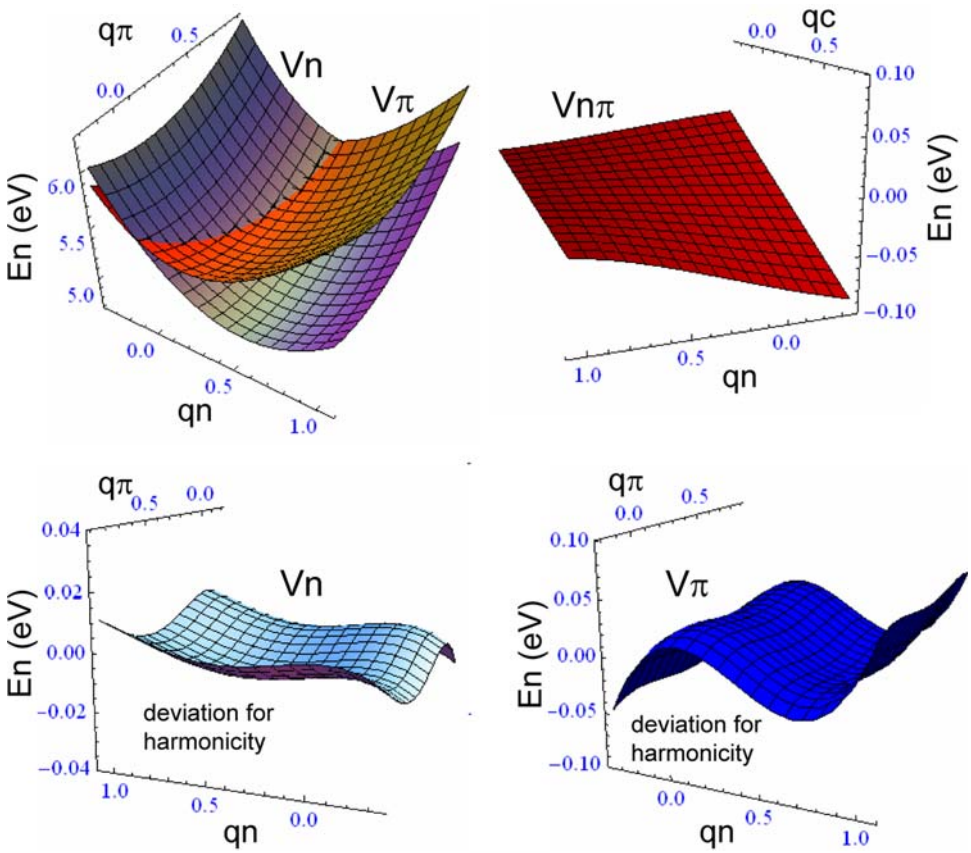

Fig. 5 $U \cdot 4H_2O$ in water. *Upper* V_n and V_π diabatic potentials (*left*) and their coupling $V_{n\pi}$ (*right*). *Lower left*/*right* difference in the fits for V_n/V_π adopting either the potentials in Table 6 or simpler quadratic forms. Coordinates are expressed in bohr $\times$ amu$^{1/2}$

and the substituent of U ring. The PESs of S_n and S_π states are very close in all the coordinate regions connecting the FC point with the minimum of the spectroscopic state S_π. In all the 3D models we have documented the existence of a crossing seam between the two excited states from which a barrierless path leads to the stable S_n minimum. Therefore, inspection of the PES strongly suggests that a $S_\pi \rightarrow S_n$ population transfer is likely. Additionally our preliminary QD results point out the necessity of a dynamical approach. In fact only such an approach can show if a population transfer occurs, what is the amount of population transferred, and what is the time-scale of the process. Furthermore, the results hereby presented show that the diabatic coupling play a fundamental role in modulating the transfer. In fact for U, both in water and CH_3CN, different choices of the coupling coordinates lead to drastically different population transfer notwithstanding the fact that the other two coordinates q_n and q_π, which are responsible for most of the coherent motion on the adiabatic PES and lead the system toward the conical intersection region, are the same. Finally, we have shown that a reduced dimensionality model is able to provide indications in very good agreement with time-resolved experiments, also when tackling medium size molecules in solution.

The approach we followed, based on a diabatic picture of the electronic surfaces, is in principle generally applicable in all the cases of non-adiabatic transitions. In practice, definition of diabatic states may become problematic in sizeable non-symmetric species, if the "diabatic" character cannot be traced back to easily computable observables, allowing the usage of property-based diabatization schemes. Nonetheless we notice that interesting attempts toward general diabatization procedures have been recently presented [52, 69]. Another aspect that can limit the applicability of our approach, concerns the definition of coordinates. The specific problem of the S_π/S_n population transfer in U derivatives can be very conveniently investigated by a model depending on the known S_0 normal coordinates, with the additional benefit of a kinetic Hamiltonian written in a very simple, diagonal, and coordinate independent expression. Different problems, involving for example large amplitude motions, may require the usage of internal coordinates and consequently more complex kinetic Hamiltonians. Moreover, in unfavorable situations, the definition itself of few main coordinates can be very troublesome. This is the case, for example, of the S_π/S_0 direct decay channel, since the corresponding conical intersection is located at highly distorted non-planar configurations, and many different internal coordinates are needed to describe the dynamics, also because of the constrains imposed by the molecular ring structure.

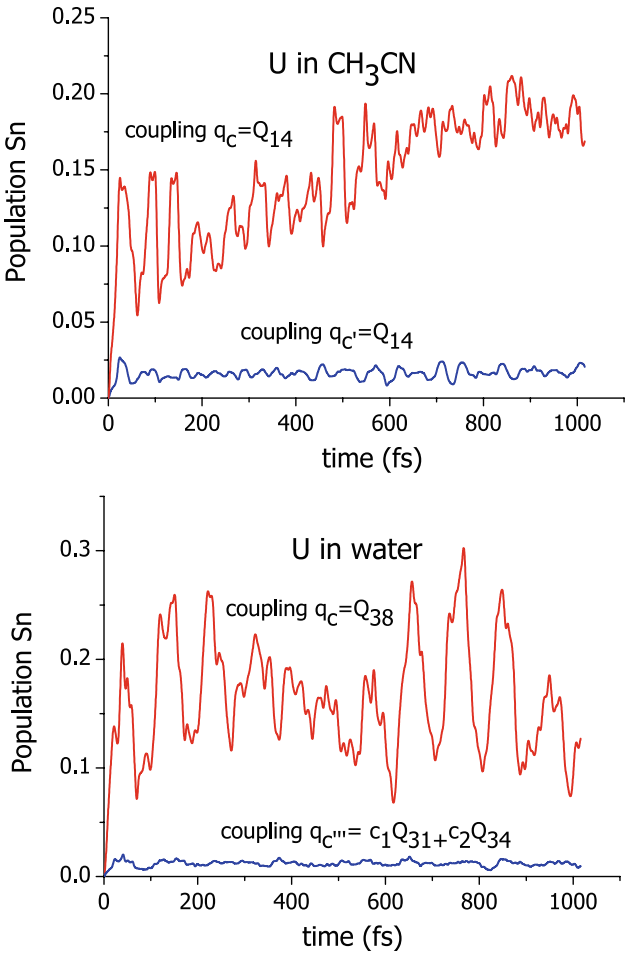

Fig. 6 Population of the S_n state as a function of time for U in CH_3CN and U · $4H_2O$ in water according to different choices of the out-of-plane coordinate that introduces the coupling in the 3D model

As we clearly stated above, our approach is suitable to reliably treat the ultrafast part of the excited state dynamics. On the other hand, including a larger number of degrees of freedom is likely necessary to study the evolution of the system on a longer timescale. In principle, the role of the nuclear degrees of freedom excluded by our model could be investigated by full-coordinate semiclassical trajectories coupled with some scheme for accounting for hopping between different electronic states [18]. However, this would require an approximate description of the core process we want to study, i.e., the non-adiabatic population transfer, and the on-the-fly evaluation of non-adiabatic couplings, not yet available in commercial TD-DFT codes. The role of other modes of the molecule could be described, still at quantum level, by resorting to multi-configurational approaches like MCTDH [14]. Of course one should then rely on a less accurate description of the PESs which cannot be computed on extended N dimensional grids and must be obtained by low-order Taylor expansions in the normal coordinates, where the coefficients are evaluated by single point calculation and numerical derivatives at some relevant points. Though we plan to go toward such a description, the analysis in Ref. [49] suggests that, for the ultrafast time scale on which we are interested, the neglected modes should not play a dominant role. Furthermore, the approximated PESs will need a careful validation and the present 3D model, taking into account anharmonicities, will be a valuable tool to investigate their role in the system dynamics and to assess to what extent they can be safely neglected.

References

1. Wang CH (1985) Spectroscopy of condensed media. Academic Press, New York
2. Fleming GR (1986) Chemical applications of ultrafast spectroscopy. Oxford University, New York
3. Assion A, Baumert T, Bergt M, Brixner T, Kiefer B, Seyfried W, Strehle M, Gerber G (1998) Science 282:919
4. Olivucci M, Sinicropi A (2005) Computational Photochemistry. In: Olivucci M (ed) Computational photochemistry, vol 16. Elsevier, Amsterdam
5. Dreuw A, Head-Gordon M (2005) Chem Rev 105:4009
6. Andersson K, Roos BO, Yarkony DR (1995) Modern Electronic Structure Theory, vol 1. World Scientific, New York, p 55
7. Barone V, Improta R, Rega N (2008) Acc Chem Res 41:605
8. Improta R, Barone V, Santoro F (2007) Angew Chem Int Ed 46:405
9. Santoro F, Improta R, Lami A, Bloino J, Barone V (2007) J Chem Phys 126:084509
10. Santoro F, Lami A, Improta R, Barone V (2007) J Chem Phys 126:184102
11. Olivucci M (2004) In: Domcke W, Yarkony DR, Koppel H (eds) Conical intersections, electronic structure, dynamics & spectroscopy. World Scientific, Singapore
12. Olivucci M, Santoro F (2008) Angew Chem Int Ed 47:6322
13. Lami A, Villani G, (2007) Theor Chem Acc 117:755
14. Meyer H-D, Manthe U, Cederbaum LS (1990) Chem Phys Lett 171:97
15. Beck H, Jäckle A, Worth G, Meyer H-D (2000) Phys Rep 324:1
16. Raab A, Worth G, Meyer H-D, Cederbaum LS (1999) J Chem Phys 110:936
17. Miller WH (2001) J Phys Chem A 105:2942
18. Tully JC (1990) J Chem Phys 93:1061
19. Granucci G, Persico M, Toniolo A (2001) J Chem Phys 114:10608
20. Frutos LM, Andruniów T, Santoro F, Ferré N, Olivucci M (2007) Proc Natl Acad Sci USA 104:7764
21. Ben-Nun M, Quenneville J, Martínez TJ (2000) J Phys Chem A 104:5161
22. Santoro F, Petrongolo C, Granucci G, Persico M (2000) Chem Phys 259:193; Chem Phys (2000) 261:489
23. Ferretti A, Granucci G, Lami A, Persico M, Villani G (1996) J Chem Phys 104:5517
24. Olivucci M, Lami A, Santoro F (2005) Angew Chem Int Ed 44:5118
25. Santoro F, Lami A, Olivucci M (2007) Theor Chem Acc 117:1061
26. Crespo-Hernandez CE, Cohen B, Hare PM, Kohler B (2004) Chem Rev 104:1977

27. Crespo-Hernandez CE, Cohen B, Kohler B (2005) Nature 436:1141; Nature (2006) 441:E8
28. Matsika S (2004) J Phys Chem A 108:7584
29. Perun S, Sobolewski AL, Domcke W (2006) J Phys Chem A 110:13238
30. Merchán M, Gonzalez-Luque R, Climent T, Serrano-Andrés L, Rodriguez E, Reguero M, Pelaez D (2006) J Phys Chem B 110:26471
31. Gustavsson T, Sarkar N, Banyasz A, Markovitsi D, Improta R (2007) Photochem Photobiol 83:595
32. Gustavsson T, Sarkar N, Lazzarotto E, Markovitsi D, Barone V, Improta R (2006) J Phys Chem B 110:12843
33. Gustavsson T, Banyasz A, Lazzarotto E, Markovitsi D, Scalmani G, Frisch MJ, Barone V, Improta R (2006) J Am Chem Soc 128:607
34. Santoro F, Barone V, Gustavsson T, Improta R (2006) J Am Chem Soc 128:16312
35. Hare PM, Crespo-Hernandez C, Kohler B (2007) Proc Natl Acad Sci USA 104:435
36. Hare PM, Crespo-Hernandez CE, Kohler B (2006) J Phys Chem B 110:18641
37. Mercier Y, Santoro F, Reguero M, Improta R, (2008) J Phys Chem B 112:10769
38. Gustavsson T, Sarkar N, Lazzarotto E, Markovitsi D, Improta R (2006) Chem Phys Lett 429:551
39. Improta R, Barone V (2004) J Am Chem Soc 126:14320
40. Improta R, Barone V (2008) Theor Chem Acc 120:491
41. Improta R (2008) Phys Chem Chem Phys 10:2656
42. Santoro F, Barone V, Improta R (2007) Proc Natl Acad Sci USA 104:9931
43. Santoro F, Barone V, Lami A, Improta R, unpublished results
44. Miertus S, Scrocco E, Tomasi J (1981) Chem Phys 55:117
45. Tomasi J, Mennucci B, Cammi R (2005) Chem Rev 105:2999
46. He Y, Wu C, Kong W (2004) J Phys Chem A 108:943
47. Chahinian M, Seba HB, Ancian B (1998) Chem Phys Lett 285:337
48. Gaigeot MP, Sprik M (2004) J Phys Chem B 108:7458
49. Gindensperger E, Cederbaum LS (2007) J Chem Phys 127:124107
50. Billinghurst BE, Yeung R, Loppnow GR (2006) J Phys Chem A 110:6185
51. Köppel H, Domcke W, Cederbaum LS (2004) In: Domcke W, Yarkony DR, Koppel H (eds) Conical Intersections, Electronic Structure, dynamics & spectroscopy, Chap 7. World Scientific Publishing, Singapore, p 323
52. Köppel H (2004) In: Domcke W, Yarkony DR, Koppel H (eds) Conical Intersections, Electronic Structure, dynamics & spectroscopy, Chap 4. World Scientific Publishing, Singapore, p 175
53. Caricato M, Ingrosso F, Mennucci B, Tomasi J (2005) J Chem Phys 122:154501
54. Burghardt I, Hynes JT (2006) J Phys Chem A 110:11411
55. Horng ML, Gardecki JA, Papazyan A, Maroncelli M (1995). J Phy Chem 99:17311
56. Dreuw A, Head-Gordon M (2005) Chem Rev 105:4009-4037
57. Burke K, Werschnik J, Gross EKU (2005) J Chem Phys 123:062206
58. Adamo C, Barone V (1999) J Chem Phys 110:6158
59. Enzerhof M, Scuseria GE (1999) J Chem Phys 110:5029
60. Adamo C, Scuseria GE, Barone V (1999) J Chem Phys 111:2889
61. Levine BG, Ko C, Quenneville J, Martínez TJ (2006) Mol Phys 104:1039
62. Cordova F, Joubert Doriol L, Ipatov A, Casida ME, Filippi C, Vela A (2007) J Chem Phys 127:164111
63. Tapavicza E, Tavernelli I, Rothlisberger U (2007) Phys Rev Lett 98:023001
64. Tapavicza E, Tavernelli I, Rothlisberger U, Filippi C, Casida ME (2008) J Chem Phys 129:124108
65. Werner U, Mitric R, Suzuki T, Bonacic-Koutecký V (2008) Chem Phys 349:319
66. Barone V, Cossi M, Tomasi J (1997) J Chem Phys 107:3210
67. Kosloff R (1996) In: Wyatt RE, Zhang JZH (eds) Dynamics of molecules and chemical reactions. Marcel Dekker Inc., New York
68. Lanczos C (1950) Res Nat Bur Stand 45:225
69. Köppel H, Schubert B (2006) Mol Phys 104:1069